ACS APPLIED MATERIALS & INTERFACES

Research Article

Cite This: ACS Appl. Mater. Interfaces 2018, 10, 11872−11879

www.acsami.org

Visual and Colorimetric High-Throughput Analysis of Chiral Carboxylic Acids Based on Enantioselective Charge Shielding of Gold Nanoparticles

Fengfeng Xie, Qing Bai, Xuemei Jiang, Xinsheng Yu, Zhining Xia, and Weili Wei*

School of Pharmaceutical Sciences and Innovative Drug Research Center, Chongqing Key Laboratory of Total Synthesis of Natural Products and Innovative Drug Research, Chongqing University, Chongqing 401331, PR China

Supporting Information

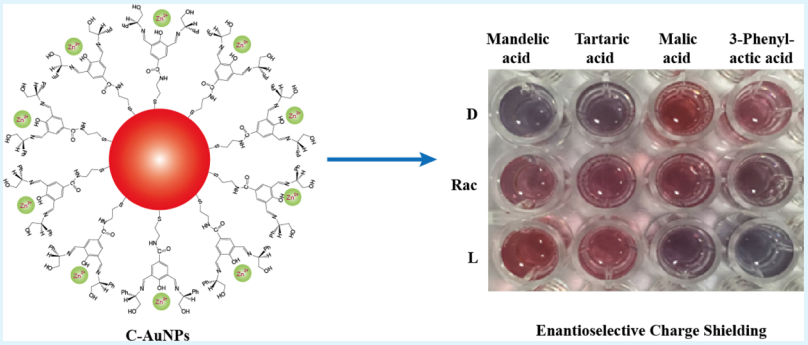

ABSTRACT: Because chiral carboxylic acids (CCAs) are a class of important biological molecules and common functional moieties found in pharmaceutical molecules, the chiral analysis of CCAs has received much attention. Herein, we developed a simple, rapid, and cost-effective method for visual and colorimetric high-throughput analysis of CCAs using chiral di-imine structure-modified gold nanoparticles (C-AuNPs) as the probe. The C-AuNPs are positively charged in the presence of zinc ion, and they can be enantioselectively shielded by the negatively charged CCA enantiomers. Therefore, upon the addition of different concentrations and enantiomeric excess (ee) of CCAs, the C-AuNP-based sensor shows the different levels of aggregation along with the visual changes in solution color, which can achieve simultaneous analysis of the concentration and ee of CCAs. The chiral recognition mechanism based on C-AuNPs was investigated by the determination of binding constants (K) and molecular simulation methods. Our approach is expected to have the wide-ranging applications in the developing region for enantio-sensing of various chiral drugs and biomolecules.

KEYWORDS: *gold nanoparticle, chiral carboxylic acid, enantioselectivity, colorimetric, high-throughput, charge shielding*

1. INTRODUCTION

Chirality plays a significant role in the activity of biological molecules and broad classes of chemical reactions, but rapid and convenient detecting and quantifying remains challenging.[1] Chiral carboxylic acids (CCAs) that are ubiquitous in nature have been intensively studied because of their fundamental roles in biological processes and drug development.[2,3] Thus, developing time-efficient and cost-effective methods for simultaneous analysis of the enantiopurity and concentration of CCAs is valuable and fascinating. To date, chromatographic and electrophoretic separation[4,5] and spectroscopic approaches[6−11] such as nuclear magnetic resonance, fluorescence, and circular dichroism (CD) spectroscopies have been widely used for analysis of CCAs. However, these methods usually have some shortcomings such as being time consuming, complicated operation, and the need for sophisticated instrumentation. Therefore, simple and cost-effective methods for high-throughput analysis of CCAs are useful.

At present, gold nanoparticles (AuNPs) have been widely used to design visual and colorimetric sensors owing to their distinctive plasmon resonance character and optical properties, which can carry out versatile chemical and biological sensing from small molecules to macromolecules and even cells.[12−15] The key to the AuNP-based sensors is the control of colloidal AuNP dispersion and aggregation states by using certain molecular recognition mechanisms specified to the analyte.[16−18] Meanwhile, AuNPs have also been explored for the construction of chiral sensors. For instance, *N*-acetyl-L-cysteine-modified AuNPs were used for colorimetric chiral sensing of tyrosine,[19] and the L-proline modified AuNPs were used to determine the enantiomeric excess (ee) of histidine.[20] But most ever reported AuNP-based chiral sensors somehow lack the insight of chiral recognition mechanism and the capability of

Received: January 4, 2018
Accepted: March 23, 2018
Published: March 23, 2018

DOI: 10.1021/acsami.8b00149
ACS Appl. Mater. Interfaces 2018, 10, 11872−11879

high-throughput analysis. In this regard, we previously reported a rationally designed protocol for high-throughput assay of both concentration and ee of chiral vicinal diols based on borate ester cross-linked AuNPs.[21]

Herein, we rationally designed and synthesized a chiral metallo-supramolecular system containing chiral di-imine structures (CDIS) and zinc ions (Zn(II)) in respect that it has a well-known binding ability to carboxylic acids.[22−24] In addition, it was reported that the CDIS bind to mandelic acid enantiomers with highly chiral selectivity.[25] Hence, the CDIS were modified onto the surface of AuNPs (namely, C-AuNPs) and subsequently formed chiral metallo-supramolecular complexes with Zn(II) for visual and colorimetric high-throughput analysis of CCAs, which has not been reported yet. As shown in Scheme 1, the AuNPs' surface metallo-supramolecular complexes could translate the chiral recognition of CCAs into visual response based on the enantioselective charge shielding-induced aggregation of C-AuNPs. The C-AuNPs showed different degrees of aggregation in the presence of different concentrations and ee of CCAs. The chiral recognition mechanism was further explored by the determination of binding constants (K) and molecular simulation methods. Our work provided a distinctive way to realize chiral analysis of CCAs with simplicity, low cost, high enantioselectivity, and high-throughput.

Scheme 1. Schematic Illustration of the Mechanism Behind Enantioselective Charge Shielding of C-AuNPs for Visual and Colorimetric High-Throughput Analysis of CCAs

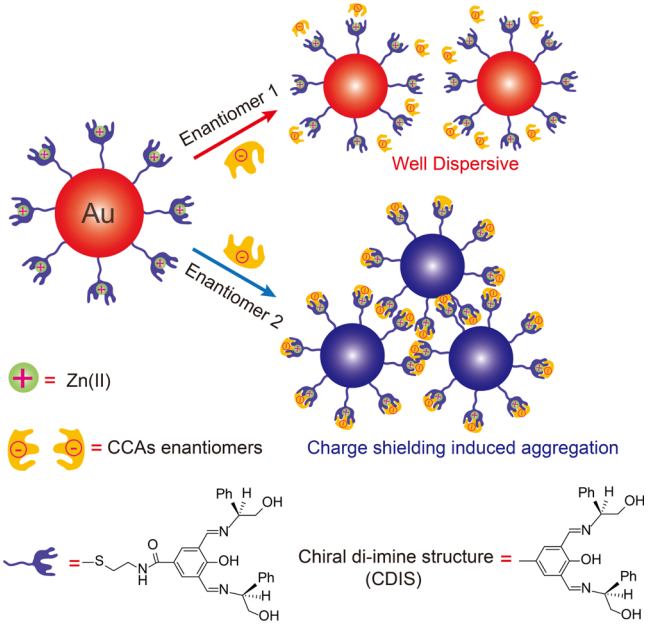

2. EXPERIMENTAL SECTION

2.1. Materials and Reagents. Chloroauric acid ($HAuCl_4$), and all enantiomers of mandelic acid, tartaric acid, malic acid, and 3-phenyllactic acid were purchased from Aladdin Chemistry Co., Ltd. (Shanghai, China). (R)-2-Amino-phenylethanol was provided from Daicel Chiral Technologies Co., Ltd. (Shanghai, China). The 2-aminoethanethiol (MEA) was purchased from Adamas-beta Chemistry Co., Ltd. (Shanghai, China). Other reagents were of analytical reagent grade and were directly used without further purification. Ultrapure water was prepared by a Millipore Milli-Q purification system and used in all experiments.

2.2. Instrumentations. Ultraviolet visible (UV−vis) absorption spectra were recorded on a Cary 8450 Spectrophotometer (Agilent, American) at room temperature. The photographs were taken with a Canon 500 digital camera. ^1H and ^{13}C nuclear magnetic resonance spectra were recorded on an Agilent 400MR DD2 400 MHz spectrometer. Electrospray ionization-mass spectrometry (ESI-MS) analysis was conducted on an ACQUITY SQD single quadrupole high-performance liquid chromatography−mass spectrometry system (Waters, USA). An ultrasonic cleaner was used to blend the solutions. The pH measurements were conducted by a PHS-3C instrument. The Fourier transform infrared (FTIR) spectra were acquired on a Shimadzu IRAffinity-1 FTIR spectrometer. Transmission electron microscopy (TEM) measurements were performed on a Zeiss LIBRA 200 FEG instrument. The samples for TEM characterization were prepared by placing a drop of colloidal solution on carbon-coated copper grid and dried at room temperature. The circular dichroism spectra were measured by Applied Photophysics Chirascan CD spectrometer. Dynamic light scattering measurements (Malvern Zetasizer Nano ZS instrument) were carried out at 25 °C under corresponding solution conditions (pH = 8).

2.3. Preparation of AuNPs. AuNPs with an average diameter of 13 nm were prepared by the citrate reduction of $HAuCl_4$ according to the reported method.[26] All glasswares used in the preparation and storage of AuNPs were cleaned in aqua regia, rinsed with ultrapure water, and dried prior to use. An aqueous solution of $HAuCl_4$ (100 mL, 1 mM) was brought to a refluxing solution quickly with rapid stirring, and then trisodium citrate solution (10 mL, 38.8 mM) was added rapidly, which resulted in the change in solution color from light yellow to dark red within ca. 1 min. The resulting solution was boiled for an additional 15 min, allowed to cool to room temperature, and further stirred, filtered through a 0.22 μm syringe filter, and stored in a refrigerator at 4 °C before the detection experiments. The concentration of the prepared AuNPs was about 10.59 nM according to Beer's law using an extinction coefficient of 2.7×10^8 M^{-1} cm^{-1} at 520 nm for 13 nm AuNPs.[27]

2.4. Synthesis of C-AuNPs. The C-AuNPs were prepared by the following procedures (Scheme S1). Accordingly, the as-prepared AuNPs were first stabilized by adding 5% TWEEN 20 to AuNP solution under stirring for 2 h. The AuNPs were first modified with MEA by mixing MEA solution with the AuNP solution at a molar ratio of 1000:1 (MEA/AuNPs) by shaking gently overnight in dark at room temperature. $NaHCO_3$ solution (6.5 mL, 10 mM) was added to 65 mL of MEA/AuNPs under stirring for 10 min (pH = 8.0). Then, N-succinimidyt-3,5-diformyl-4-hydroxybenzoate (18 mL, 0.42 mM) in ethanol was added drop by drop under stirring for 13 h. The obtained amide-AuNPs were concentrated by several cycles of centrifugation, decantation, and redispersion in ethanol/water (1:4). Finally, the C-AuNPs were prepared by mixing (R)-2-amino-phenylethanol (100 μM) with the amide-AuNPs (10 nM) at pH = 8.0 with stirring for 2 h at room temperature.[28] The C-AuNPs were purified for further use through centrifugation, decantation, and redispersion. The solution pH was adjusted to 9.0 with NaOH to prevent hydrolysis of C═N bond. C-AuNP solution was freeze-dried for long-term storage in the refrigerator at 4 °C.

2.5. Visual and Colorimetric High-Throughput Analysis of CCAs. For the enantioselectivity assay of C-AuNPs, the C-AuNPs (100 μL, 10 nM), $ZnCl_2$ (100 μL, 100 μM), and mandelic acid solution (100 μL) were mixed in a well of a 96-well plate. Then, the mixed solution was incubated for 30 min at room temperature (ca. 25 °C). The total volume of the mixture was 300 μL, and the final concentration of mandelic acid was 0.9 mM. The solution in the plate well was used for visual investigation. The mixture in each plate well was diluted to 2.8 mL (for 3 mL cuvette) for measurements of UV−vis absorption spectra by the UV−vis spectrophotometer.

A standard plate was made with C-AuNPs and achiral AuNPs for the high-throughput analysis of total concentration and ee of mandelic acid. The C-AuNPs or achiral AuNPs (50 μL, 10 nM), $ZnCl_2$ (50 μL, 100 μM) and mandelic acid solution (50 μL) with appropriate concentration were successively added to each microwell of the Corning 96-well polystyrene plates. The prepared plate was sealed to

DOI: 10.1021/acsami.8b00149
ACS Appl. Mater. Interfaces 2018, 10, 11872−11879

prevent solvent evaporation and was incubated for 30 min at room temperature (ca. 25 °C). The standard total concentration titration of mandelic acid was carried out at seven different concentrations (0.1, 0.2, 0.4, 0.6, 0.8, 1.0, and 1.2 mM) with achiral AuNPs. The standard ee titrations of mandelic acid were carried out at seven different concentrations (0.1, 0.2, 0.4, 0.6, 0.8, 1.0, and 1.2 mM) and 11 different D-mandelic acid ee values (−100, −80, −60, −40, −20, 0, 20, 40, 60, 80, and 100) % with C-AuNPs. The absorbance values at 520 and 626 nm of each microwell of the standard plate were recorded by a plate reader.

A screening plate was designed with C-AuNPs for evaluating the generality of C-AuNP sensing for visual and colorimetric analysis of CCAs. The four CCAs, mandelic acid, tartaric acid, malic acid, and 3-phenyllactic acid, were chosen for analysis. The enantiomers and raceme of 0.9 mM mandelic acid, 0.5 mM tartaric acid, 0.4 mM malic acid, and 1.0 mM 3-phenyllactic acid were tested to C-AuNP solution containing $ZnCl_2$. The color changes of the solutions were observed and recorded using a digital camera.

The mass ratio of Zn/Au was determined to be 0.0109 by inductively coupled plasma mass spectrometry. According to a previously reported method, the mole ratio of CDIS/AuNPs was calculated to be 947:1.[29] In other words, the average number of CDIS on each AuNP was about 947 in the present work. Because the number of CDIS modified on AuNPs' surface was about 10^3 times more than the number of AuNPs, the concentration of CCA solution was about 10^3 times higher than the concentration of CDIS. All solutions were made with the mixture of aqueous solution containing 20 vol % methanol (pH = 9).

2.6. Molecular Simulation. A representative docking method was used to further study the interaction between CDIS−Zn(II) complexes and CCAs, namely, CDOCKER, a molecular dynamics (MD) simulated-annealing-based algorithm.[30] The CCA as a ligand was docked into the binding site of the CDIS−Zn(II) complex. Random ligand conformations were generated by high-temperature MD. After the conformations were translated into the binding site, the candidate poses were created using random rigid-body rotations followed by simulated annealing. A final minimization was used to refine the ligand poses.

3. RESULTS AND DISCUSSION

3.1. Characterization of C-AuNPs. The as-prepared AuNPs were modified via a step-by-step route forming MEA-, amide-, and C-AuNPs, consecutively (Scheme S1). In brief, the as-prepared AuNPs were first covalently modified with MEA through the well-known S−Au bond, and then C-AuNPs were obtained by amidation and nucleophilic addition reactions. As shown in Figure 1A, the maximum absorption peaks of the UV−vis spectra of AuNPs and C-AuNPs were at 520 and 525 nm, respectively. The peak red shift and broadening of the UV−vis spectrum of C-AuNPs should be due to the slight aggregation resulting from weak interactions such as $\pi-\pi$, hydrophobic interactions after CDIS were modified on the surface of AuNPs. However, the color of C-AuNP solution was still wine red, and there was no obvious difference compared with the color of AuNP solution (inset of Figure 1A). The monodispersion state of C-AuNPs was also proved by the TEM image (Figure 1B). The FTIR spectra were performed to further confirm the step-by-step modification of C-AuNPs (Figure 1C). In the spectrum of MEA/AuNPs, the peak characteristics of MEA were observed at 1086, 1640, and 3305 cm^{-1}, corresponding to υ(C−N), δ(N−H), and υ(N−H), respectively. The spectrum of amide-AuNPs showed the peaks at 1096, 1647, 1735, and 3302 cm^{-1} corresponding to υ(C−O), υ(C═O) of amide group, υ(C═O) of aldehyde group, and υ(O−H), respectively. Similarly, the spectrum of C-AuNPs exhibited its main characteristic peak at 1667 cm^{-1} corresponding to υ(C═N), indicating the formation of CDIS on nanoparticle surface. As we all know, some nonaromatic imine (C═N) structures are not stable under aqueous conditions. Therefore, the chemical stability of CDIS on the surface of C-AuNPs was investigated. As shown in Figure S1, CDIS were stable within at least 24 h in water solution at pH 9. This result was reasonable as the CDIS were aromatic imines. Therefore, all subsequent experiments were conducted at pH 9.

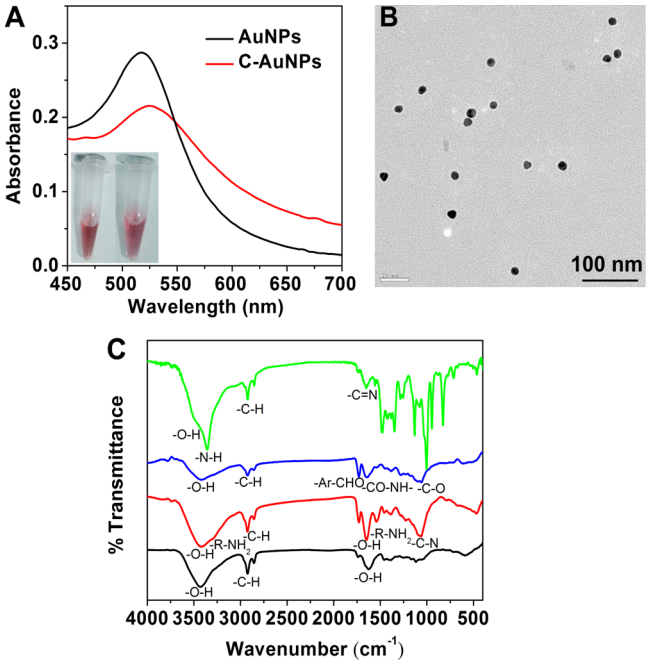

Figure 1. (A) UV−vis absorption spectra of the AuNPs and C-AuNPs (13 nm). The AuNP and C-AuNP solution showed wine red in the inset. (B) TEM image of C-AuNPs (13 nm). (C) FTIR spectra of AuNPs (black), MEA/AuNPs (red), amide-AuNPs (blue), and C-AuNPs (green).

3.2. Enantioselectivity of C-AuNPs to Mandelic Acid. To investigate the enantioselective ability of C-AuNPs in the presence of Zn(II) for CCAs, mandelic acid was chosen as a model. The UV−vis absorption spectra of C-AuNPs responding to the different concentration of L-mandelic acid or D-mandelic acid were obtained (Figure S2). Under the same concentration, D-mandelic acid induced more obvious red shift of plasmon resonance band of C-AuNPs compared with L-mandelic acid. A representative enantioselective assembly of C-AuNPs with mandelic acid enantiomers is shown in Figure 2A. As expected, in the presence of 0.9 mM D-mandelic acid, the absorbance at 520 nm decreased, and it was noteworthy that a new absorbance peak emerged at 626 nm in contrast to the spectrum of original C-AuNPs, suggesting the aggregation of C-AuNPs. However, the spectrum responding to 0.9 mM L-mandelic acid had no significant change compared with that of original C-AuNPs (Figure 2B). Meanwhile, the corresponding TEM images clearly showed that D-mandelic acid could selectively induce aggregation of C-AuNPs (Figure 2C). The dynamic light scattering measurements were further performed as shown in Figure S4. The average hydrodynamic diameters (D_H) of as-prepared AuNPs and C-AuNPs were 15.5 and 17.6 nm, respectively. In addition, the hydrodynamic diameter distribution of C-AuNPs was wider than that of as-prepared AuNPs, indicating that there was the slight aggregation resulting from weak interactions such as $\pi-\pi$, hydrophobic

DOI: 10.1021/acsami.8b00149
ACS Appl. Mater. Interfaces 2018, 10, 11872−11879

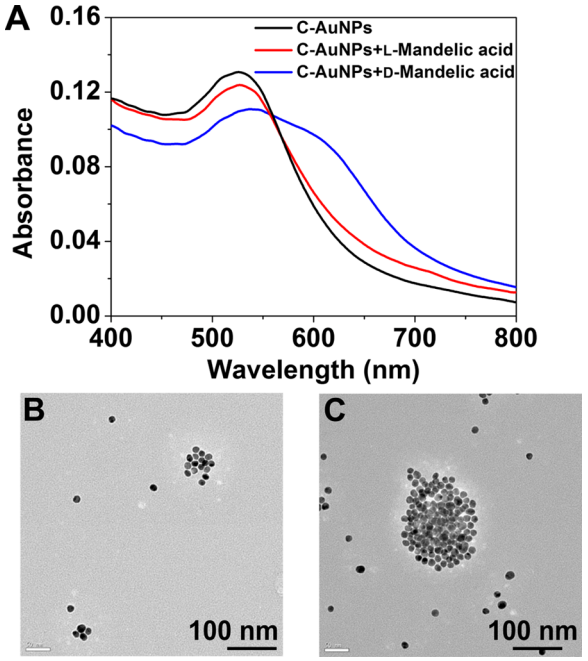

Figure 2. (A) UV−vis absorption spectra of C-AuNPs, C-AuNPs in the presence of 0.9 mM L-mandelic acid or D-mandelic acid with 100 μM $ZnCl_2$. (B) Corresponding TEM images of C-AuNPs/Zn(II) in the presence of L-mandelic acid (B) and D-mandelic acid (C).

interactions after CDIS were modified on the surface of AuNPs. Furthermore, the D_H in the presence of the same concentration D- and L-mandelic acid was 51.3 and 167.2 nm, respectively, which confirmed that the aggregation of AuNPs caused by D-/L-mandelic acid and showed that obvious difference in the whole solution and D-mandelic acid could selectively induce the aggregation of C-AuNPs. These results proved that our designed C-AuNPs had obvious enantioselectivity for mandelic acid.

Besides, the enantioselective ability of C-AuNPs without zinc ions was investigated as shown in Figure S3; in the absence of zinc ions, the response sensitivity of C-AuNP solution to mandelic acid enantiomers was very low and had no enantioselectivity. Therefore, zinc ions were added to the C-AuNP solution, forming a chiral metallo-supramolecular system for the enantioselective recognition and analysis of CCAs in subsequent experiments.

Zeta potential (ζ) measurements were further carried out to understand the reason of C-AuNP aggregation in the presence of CCAs. The initial ζ of C-AuNPs in the presence of 100 μM Zn(II) was measured to be +20 mV. Obviously, the ζ of C-AuNPs was decreased to +0.5 and +17 mV after the addition of 0.9 mM D- or L-mandelic acid, respectively. The decrease of ζ should be due to charge shielding of the positively charged C-AuNPs + Zn(II) system after binding with the negatively charged carboxylic acids. The results proved the enantioselective charge shielding-induced aggregation of C-AuNPs as shown in Scheme 1.

3.3. High-Throughput Chiral Analysis of Mandelic Acid with C-AuNPs. After succeeding in the test of enantioselective recognition properties of C-AuNPs, the simultaneous analysis of total concentration ($[acid]_t$) and ee of mandelic acid was investigated. Herein, an achiral AuNP (aC-AuNPs) probe was prepared for $[acid]_t$ determination according to our previous work.[21] Similar to the C-AuNPs, the aC-AuNPs were prepared by simply replacing the chiral amine with achiral phenylethylamine (Scheme S2). Because the aC-AuNPs were achiral, they became unresponsive to chirality and only responded to the concentration. As shown in Figure S5A, the UV−vis absorption spectra of aC-AuNPs responding to the same 0.8 mM D-mandelic acid or L-mandelic acid were identical. Upon the addition of seven different concentrations of D-mandelic acid, the absorption spectra of aC-AuNPs showed red shift in varying degrees, suggesting the different levels of aC-AuNP aggregation (Figure S5B). On the other hand, because the C-AuNPs were chiral and had the high enantioselectivity for CCAs, C-AuNPs were used for the quantitative analysis of ee, and then the concentration of each enantiomer could be acquired by calculation according to the $[acid]_t$ and ee values of CCAs.

Next, a standard plate with aC-AuNPs and C-AuNPs was made for the high-throughput analysis of both $[acid]_t$ and ee of mandelic acid. Because the aggregation of AuNPs generally resulted in a significant increase in the absorbance at 626 nm (A_{626}) and decrease in the absorbance at 520 nm (A_{520}), the ratio of A_{520} to A_{626} (A_{520}/A_{626}) was chosen to reflect the assembly of C-AuNPs.[31,32] A lower ratio corresponded to assembled clusters of C-AuNPs and the color of the solution was blue, whereas a higher ratio referred to dispersed C-AuNPs and the color of the solution was red. The A_{520}/A_{626} signals of each microwell of the standard plate recorded by a plate reader for the $[acid]_t$ and ee values of mandelic acid as described above are shown in Figure 3. As commonly adopted in the previous

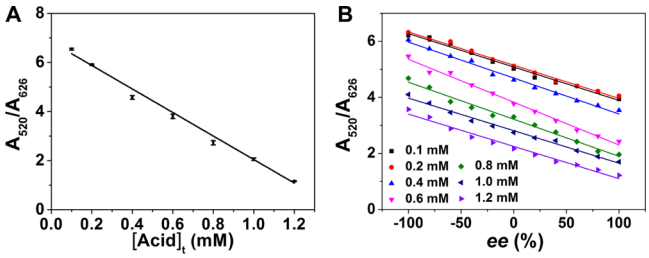

Figure 3. Analysis of the standard plate. (A) Standard $[acid]_t$ titration of aC-AuNPs at seven different concentration (0.1, 0.2, 0.4, 0.6, 0.8, 1.0, and 1.2 mM) of mandelic acid containing $ZnCl_2$. (B) Standard ee titration of C-AuNPs at seven different $[acid]_t$ (0.1, 0.2, 0.4, 0.6, 0.8, 1.0, and 1.2 mM) and 11 different D-mandelic acid ee values (−100, −80, −60, −40, −20, 0, 20, 40, 60, 80, and 100) %. All measurements were taken at 25 °C. Error bars were obtained from three experiments.

assays,[33,34] the A_{520}/A_{626} values from ee and $[acid]_t$ titrations were linearly fitted against $[acid]_t$ and ee, respectively. The linear fitting results were satisfying (correlation coefficients $R^2 >$ 0.99). Consequently, it was demonstrated that the C-AuNP probe was capable of realizing high-throughput and simultaneous analysis of both $[acid]_t$ and ee of mandelic acid.

On the basis of the above results, our method can be used for the determination of $[acid]_t$ and ee of unknown samples. First, an "analysis plate" with aC-AuNPs and C-AuNPs was made, where the unknown samples with varying $[acid]_t$ and ee were tested. By monitoring the A_{520}/A_{626} values, the $[acid]_t$ and ee values of the unknown samples can be predicted according to the standard equations generated from the standard plate.

Overall, the method using C-AuNPs for simultaneous analysis of both $[acid]_t$ and ee of CCAs is rapid once a standard plate has been developed for a particular analyte. Among all procedures, loading of the AuNPs, $ZnCl_2$, and

DOI: 10.1021/acsami.8b00149
ACS Appl. Mater. Interfaces 2018, 10, 11872−11879

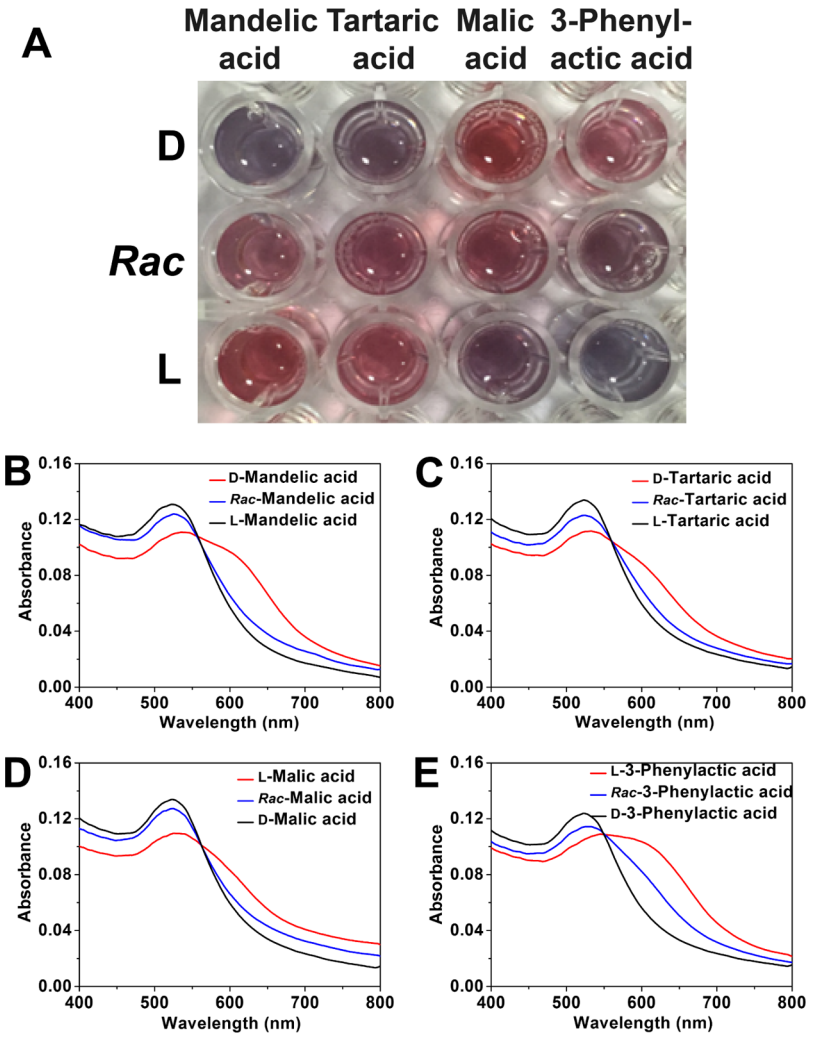

Figure 4. (A) Image of C-AuNPs responding to enantiomers and raceme of four carboxyl acids in the screening plate. The UV−vis absorption spectra of C-AuNPs responding to the enantiomers and raceme of 0.9 mM mandelic acid (B), 0.5 mM tartaric acid (C), 0.4 mM malic acid (D), and 1.0 mM 3-phenyllactic acid (E) corresponding to the screening plate. All solutions were made in the mixture of aqueous solutions containing 20 vol % methanol (pH 9). All measurements were taken at 25 °C. The *rac*-represent racemes.

unknown sample solutions to the 96-well plate requires about 30 min per 96 samples. After that, the $[acid]_t$ and ee values of 96 unknown samples can be predicted within 10 min, including about 5 min for the 96-well plate reader to record the absorbance of 96 unknowns samples at two wavelengths (520 and 626 nm) and 5 min for data analysis with a computer program.

3.4. Investigation of Generality. To evaluate the generality of C-AuNP sensing for visual and colorimetric analysis of CCAs, the four different CCAs, mandelic acid, tartaric acid, malic acid, and 3-phenyllactic acid, were selected as analytes. A screening plate was made for monitoring the colorimetric responses of C-AuNPs in the presence of enantiomers and raceme of four carboxyl acids. As shown in Figure 4A, the C-AuNPs responding to the enantiomers and raceme of each CCA presented visual color changes ranging from wine red to blue, which could be directly observed by the naked eyes. The corresponding results of UV−vis absorption spectra (Figure 4B−E) were absolutely in accordance with the results of colorimetric responses in Figure 4A, indicating that the C-AuNPs sensing could commonly apply to the visual and colorimetric analysis of diversified CCAs.

3.5. Mechanism Investigation. To figure out the mechanism based on C-AuNPs for the chiral recognition of carboxylic acids, the binding constants (K) between enantiomers of each CCA and the chiral metallo-supramolecular system (CDIS−Zn(II)) were determined by fluorescence titration. Fluorescence intensity at 635 nm of CDIS−Zn(II) with different concentrations of D-mandelic acid or L-mandelic acid containing $ZnCl_2$ affords data which can be effectively used to extract K assuming 1:1 binding, in conjunction with the modified Benesi−Hildebrand type equation,[35,36] $1/\Delta I = 1/\Delta I_{max} + (1/KC)(1/\Delta I_{max})$, in which $\Delta I = I_x - I_0$ and $\Delta I_{max} = I_\infty - I_0$; I_0, I_x, and I_∞ are the fluorescence intensities of CDIS−Zn(II) in the absence of mandelic acid, at an intermediate mandelic acid concentration and at a concentration of complete interaction, respectively and C is the mandelic acid concentration. As shown in Figure 5A, the values of $[1/(I - I_0)]$ showed a linear relationship with the change of $1/[C]$ (R^2 = 0.984), which verified the 1:1 stoichiometry between CDIS−Zn(II) complexes and CCAs on the base of the linear Benesi−Hildebrand expression. The binding constants (K) between CDIS−Zn(II) and D-/L-mandelic acid enantiomers were determined as 5.16×10^7 and 1.17×10^7 M^{-1}, respectively.

DOI: 10.1021/acsami.8b00149
ACS Appl. Mater. Interfaces 2018, 10, 11872−11879

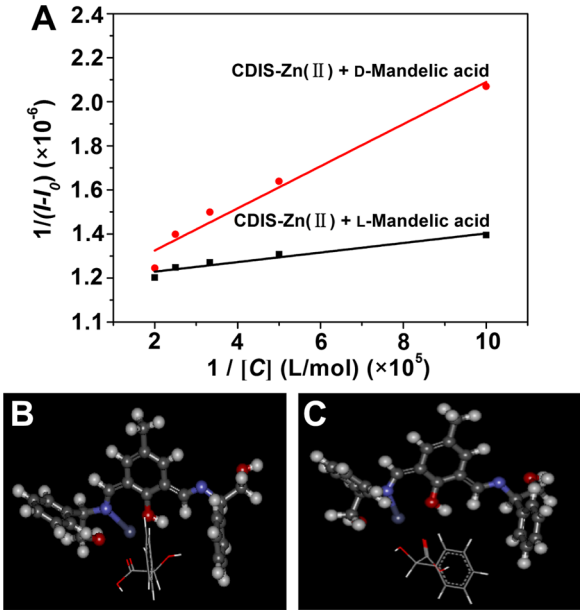

Figure 5. (A) Benesi−Hildebrand plot of 2 mM CDIS in the presence of D-mandelic acid (red) and L-mandelic acid (black) containing $ZnCl_2$ (1.0×10^{-4} M in CH_3OH). (I_0: fluorescence intensity of the sensor in the absence of mandelic acid, I: fluorescence intensity of the sensor in the presence of mandelic acid.) The docking results of CDIS−Zn(II) complex with D-mandelic acid (B) and L-mandelic acid (C). The balls in dark gray, red, blue, white, and purple refer to C, O, N, and H atoms, and Zn(II) ion, respectively.

The former is 4.4 times of the latter. The result suggested that the CDIS−Zn(II) more easily bind to D-mandelic acid because of the stereochemical difference, which further gave rise to more effective charge shielding of C-AuNPs by D-mandelic acid. This was consistent with results shown in Figure 4. The K values between CDIS−Zn(II) and the other CCAs enantiomers were similarly determined by fluorescence titration, and they are listed in Table 1.

Table 1. Results of the K and CE Between CDIS−Zn(II) and Four Pairs of CCAs Enantiomers

carboxylic acids	K ($\times 10^7$ M^{-1})	CE (kJ/mol)
D-mandelic acid	5.16	−24.4734
L-mandelic acid	1.17	−21.2552
D-tartaric acid	13.1	−30.5887
L-tartaric acid	8.14	−27.6778
D-malic acid	15.6	−33.7353
L-malic acid	17.8	−34.1749
D-3-phenyllactic acid	6.12	−25.1070
L-3-phenyllactic acid	6.88	−25.7754

To give further insights of chiral recognition mechanisms of CCAs by CDIS−Zn(II), molecular simulations were carried by using a molecular docking method.[37] The final docking results of CDIS−Zn(II) and the CCA enantiomers are shown in Figures 5 and S6. The two imine bonds, one hydroxyl group, bilateral benzene rings, and Zn(II) of CDIS−Zn(II) complex formed an inclusion cavity. Both D-mandelic acid and L-mandelic acid entered into the inclusion cavity. It was observed that the chiral center of D-mandelic acid (Figure 5B) was closer to the chiral center of CDIS compared with L-mandelic acid (Figure 5C). Although the benzene ring of D-mandelic acid was parallel to unilateral benzene ring of CDIS, there was no the repulsive interaction. Because the carbon chain of mandelic acid molecule was short, the D-mandelic acid molecule only interacted with the one side of nonparallel imine structure of CDIS. However, the benzene ring of L-mandelic acid was parallel to the middle benzene ring of CDIS, resulting in the steric hindrance and strong repulsive interaction. Besides, it is commonly acknowledged that the smaller the CDOCKER energy (CE) of the docking result, the better the pose of the interaction is. As shown in Table 1, the CE of D-mandelic acid was smaller than one of L-mandelic acid. In other words, the interaction of CDIS−Zn(II) complex and D-mandelic acid was stronger and the docking structure was more stable. The data of CE between the CDIS−Zn(II) and all CCAs enantiomers were wholly in agreement with the results of K and C-AuNPs colorimetric responses.

Furthermore, the CD spectra of the C-AuNPs and the chiral recognition between the C-AuNPs and CCAs were measured to get a full understanding of the chiral recognition mechanism. As shown in Figure S7, the spectrum of C-AuNPs exhibited two significant CD singles at 331 and 420 nm, which revealed that CDIS were successfully modified on the surface of AuNPs and C-AuNPs is chiral. Upon the addition of Zn(II) ions, compared with the spectrum of C-AuNPs, the location of peaks showed noticeable changes and the spectrum of C-AuNPs/Zn(II) exhibited two strong CD singles at 297 and 389 nm because the chelation of CDIS and zinc ions forming a chiral metallo-supramolecular complex gave rise to conformational change.

In the presence of D-mandelic acid, D-tartaric acid, L-malic acid, or L-3-phenyllactic acid, the CD single at 389 nm obviously decreased and two CD singles emerged at 339 and 423 nm in contrast to the spectrum of C-AuNPs/Zn(II) complex (Figure S7), suggesting the interaction of C-AuNPs and CCAs. In addition, the signal changes caused by D-mandelic acid, D-tartaric acid were more obvious than that by L-malic acid or L-3-phenyllactic acid, indicating the stronger interaction between C-AuNPs/Zn(II) complex and D-mandelic acid/D-tartaric acid. However, the spectra responding to L-mandelic acid, L-tartaric acid, D-malic acid, or D-3-phenyllactic acid had no significant change compared with that of C-AuNPs/Zn(II) complex, which further confirmed the enantioselective recognition of C-AuNPs for CCAs. These results were in accordance with the results of K, molecular simulation, and colorimetric responses.

According to the above results, it was revealed that the mechanism based on C-AuNPs for visual and colorimetric high-throughput analysis of CCAs was the enantioselective charge shielding forming the AuNPs' surface CDIS−Zn(II) complexes with positive charges and the CCAs with negative charges. CDIS on the surface of AuNPs first coordinated with Zn(II) ions at the ratio of 1:1 forming the CDIS−Zn(II) complexes with positive charges. By this time, C-AuNPs maintained a well monodispersed state because of sufficient positive charge repulsion. Upon the addition of CCAs with negative charges, positive charges of the C-AuNP surface were shielded and the repulsive force among C-AuNPs was weakened, which led to the aggregation of C-AuNPs along with the visual color change of the solution. Interestingly, CDIS−Zn(II) on the surface of AuNPs showed high enantioselectivity for CCAs enantiomers owing to the stereochemical difference, resulting in obvious enantioselective charge shielding and the consequent aggregation degree of C-AuNPs. Therefore, our designed method using

DOI: 10.1021/acsami.8b00149
ACS Appl. Mater. Interfaces 2018, 10, 11872−11879

C-AuNPs can realize the visual and colorimetric high-throughput analysis for CCAs.

4. CONCLUSIONS

In conclusion, a simple, cost-effective, and rapid colorimetric method for visual high-throughput analysis of CCAs using chiral metallo-supramolecular system functionalized AuNPs has been exploited in this work. The C-AuNP sensing has an ability of high enantioselective recognition for various CCAs and can realize high-throughput and simultaneous analysis of the $[acid]_t$ and ee of CCAs. The chiral recognition mechanism based on C-AuNPs is the enantioselective charge shielding forming the C-AuNPs/Zn(II) system with positive charges and CCAs with negative charges. The improvement of sensitivity of C-AuNP sensing is underway. The method using C-AuNP sensing shows the potential application in the analysis of chiral drugs.

■ ASSOCIATED CONTENT

Supporting Information

The Supporting Information is available free of charge on the ACS Publications website at DOI: 10.1021/acsami.8b00149.

Schematic depiction of the synthetic procedure of C-AuNPs; additional scheme of the mechanism for the achiral aC-AuNPs-based determination of $[acid]_t$ of carboxylic acids; UV−vis spectra of CDIS under different pH condition; UV−vis spectra of C-AuNPs responding to the different concentration of mandelic acid; UV−vis spectra of aC-AuNPs responding to mandelic acid; additional docking results of CDIS−Zn(II) complex and carboxylic acid enantiomers; and ^{1}H NMR, ^{13}C NMR, and ESI-MS characterization (PDF)

■ AUTHOR INFORMATION

Corresponding Author

*E-mail: wlwei@cqu.edu.cn.

ORCID

Weili Wei: 0000-0001-6363-3591

Author Contributions

The manuscript was written through contributions of all authors. All authors have given approval to the final version of the manuscript.

Notes

The authors declare no competing financial interest.

■ ACKNOWLEDGMENTS

This work was financially supported by the National Natural Science Foundation of China (no. 21675016), Chongqing Basic and Frontier Research Program (no. cstc2016jcyjA0328), the Fundamental Research Funds for the Central Universities of China (nos. 106112016CDJZR135505, 106112017CDJQJ238815), and the 100 Young Plan by Chongqing University (no. 0236011104410).

■ REFERENCES

(1) Patterson, D.; Schnell, M.; Doyle, J. M. Enantiomer-specific detection of chiral molecules via microwave spectroscopy. *Nature* **2013**, *497*, 475−477.

(2) Hashimoto, T.; Gálvez, A. O.; Maruoka, K. In situ assembled boronate ester assisted chiral carboxylic acid catalyzed asymmetric trans-aziridinations. *J. Am. Chem. Soc.* **2013**, *135*, 17667−17670.

(3) Lu, P.; Jackson, J. J.; Eickhoff, J. A.; Zakarian, A. Direct enantioselective conjugate addition of carboxylic acids with chiral lithium amides as traceless auxiliaries. *J. Am. Chem. Soc.* **2015**, *137*, 656−659.

(4) Hoffmann, C. V.; Pell, R.; Lämmerhofer, M.; Lindner, W. Synergistic Effects on Enantioselectivity of Zwitterionic Chiral Stationary Phases for Separations of Chiral Acids, Bases, and Amino Acids by HPLC. *Anal. Chem.* **2008**, *80*, 8780−8789.

(5) Reetz, M. T.; Kühling, K. M.; Deege, A.; Hinrichs, H.; Belder, D. Super-High-Throughput Screening of Enantioselective Catalysts by Using Capillary Array Electrophoresis. *Angew. Chem.* **2000**, *39*, 3891−3893.

(6) Joyce, L. A.; Maynor, M. S.; Dragna, J. M.; da Cruz, G. M.; Lynch, V. M.; Canary, J. W.; Anslyn, E. V. A simple method for the determination of enantiomeric excess and identity of chiral carboxylic acids. *J. Am. Chem. Soc.* **2011**, *133*, 13746−13752.

(7) Mei, X.; Wolf, C. Enantioselective Sensing of Chiral Carboxylic Acids. *J. Am. Chem. Soc.* **2004**, *126*, 14736−14737.

(8) Yang, D.; Li, X.; Fan, Y.-F.; Zhang, D.-W. Enantioselective Recognition of Carboxylates: A Receptor Derived from α-Aminoxy Acids Functions as a Chiral Shift Reagent for Carboxylic Acids. *J. Am. Chem. Soc.* **2005**, *127*, 7996−7997.

(9) Xiong, J.-B.; Xie, W.-Z.; Sun, J.-P.; Wang, J.-H.; Zhu, Z.-H.; Feng, H.-T.; Guo, D.; Zhang, H.; Zheng, Y.-S. Enantioselective Recognition for Many Different Kinds of Chiral Guests by One Chiral Receptor Based on Tetraphenylethylene Cyclohexylbisurea. *J. Org. Chem.* **2016**, *81*, 3720−3726.

(10) Li, D.-M.; Wang, H.; Zheng, Y.-S. Light-emitting property of simple AIE compounds in gel, suspension and precipitates, and application to quantitative determination of enantiomer composition. *Chem. Commun.* **2012**, *48*, 3176−3178.

(11) Liu, N.-N.; Song, S.; Li, D.-M.; Zheng, Y.-S. Highly sensitive determination of enantiomeric composition of chiral acids based on aggregation-induced emission. *Chem. Commun.* **2012**, *48*, 4908−4910.

(12) Guo, Y.; Wang, Z.; Qu, W.; Shao, H.; Jiang, X. Colorimetric detection of mercury, lead and copper ions simultaneously using protein-functionalized gold nanoparticles. *Biosens. Bioelectron.* **2011**, *26*, 4064−4069.

(13) Lee, K.; Drachev, V. P.; Irudayaraj, J. DNA−Gold Nanoparticle Reversible Networks Grown on Cell Surface Marker Sites: Application in Diagnostics. *ACS Nano* **2011**, *5*, 2109−2117.

(14) Tokonami, S.; Shiigi, H.; Nagaoka, T. Open Bridge-Structured Gold Nanoparticle Array for Label-Free DNA Detection. *Anal. Chem.* **2008**, *80*, 8071−8075.

(15) Wu, Y.; Huang, J.; Yang, X.; Yang, Y.; Quan, K.; Xie, N.; Li, J.; Ma, C.; Wang, K. Gold Nanoparticle Loaded Split-DNAzyme Probe for Amplified miRNA Detection in Living Cells. *Anal. Chem.* **2017**, *89*, 8377−8383.

(16) Li, R.-D.; Yin, B.-C.; Ye, B.-C. Ultrasensitive, colorimetric detection of microRNAs based on isothermal exponential amplification reaction-assisted gold nanoparticle amplification. *Biosens. Bioelectron.* **2016**, *86*, 1011−1016.

(17) Sankoh, S.; Thammakhet, C.; Numnuam, A.; Limbut, W.; Kanatharana, P.; Thavarungkul, P. 4-mercaptophenylboronic acid functionalized gold nanoparticles for colorimetric sialic acid detection. *Biosens. Bioelectron.* **2016**, *85*, 743−750.

(18) Liu, Y.; Han, X.; He, L.; Yin, Y. Thermoresponsive assembly of charged gold nanoparticles and their reversible tuning of plasmon coupling. *Angew. Chem., Int. Ed.* **2012**, *51*, 6373−6377.

(19) Su, H.; Zheng, Q.; Li, H. Colorimetric detection and separation of chiral tyrosine based on N-acetyl-l-cysteine modified gold nanoparticles. *J. Mater. Chem.* **2012**, *22*, 6546.

(20) Seo, S. H.; Kim, S.; Han, M. S. Gold nanoparticle-based colorimetric chiral discrimination of histidine: application to determining the enantiomeric excess of histidine. *Anal. Methods* **2014**, *6*, 73−76.

(21) Wei, W.; Wu, L.; Xu, C.; Ren, J.; Qu, X. A general approach using spiroborate reversible cross-linked Au nanoparticles for visual high-throughput screening of chiral vicinal diols. *Chem. Sci.* **2013**, *4*, 1156−1162.

DOI: 10.1021/acsami.8b00149
ACS Appl. Mater. Interfaces 2018, 10, 11872−11879

(22) Huang, Z.; Yu, S.; Wen, K.; Yu, X.; Pu, L. Zn(ii) promoted dramatic enhancement in the enantioselective fluorescent recognition of functional chiral amines by a chiral aldehyde. *Chem. Sci.* **2014**, *5*, 3457−3462.
(23) Ingold, C. K.; Weaver, S. D. LIX.—The additive formation of four-membered rings. Part VI. The addition of azo-compounds to ethylenes and some transformations of the dimethylene-1:2-di-imine ring. *J. Chem. Soc., Trans.* **1925**, *127*, 378−387.
(24) Rao, C. N. R.; Natarajan, S.; Vaidhyanathan, R. Metal Carboxylates with Open Architectures. *Angew. Chem., Int. Ed.* **2004**, *43*, 1466−1496.
(25) Dhara, K.; Sarkar, K.; Roy, P.; Nandi, M.; Bhaumik, A.; Banerjee, P. A highly enantioselective chiral Schiff-base fluorescent sensor for mandelic acid. *Tetrahedron* **2008**, *64*, 3153−3159.
(26) Brewer, S. H.; Glomm, W. R.; Johnson, M. C.; Knag, M. K.; Franzen, S. Probing BSA Binding to Citrate-Coated Gold Nanoparticles and Surfaces. *Langmuir* **2005**, *21*, 9303−9307.
(27) Jin, R.; Wu, G.; Li, Z.; Mirkin, C. A.; Schatz, G. C. What Controls the Melting Properties of DNA-Linked Gold Nanoparticle Assemblies? *J. Am. Chem. Soc.* **2003**, *125*, 1643−1654.
(28) Huc, I.; Lehn, J.-M. Virtual combinatorial libraries: Dynamic generation of molecular and supramolecular diversity by self-assembly. *Proc. Natl. Acad. Sci. U.S.A.* **1997**, *94*, 2106−2110.
(29) Volkert, A. A.; Subramaniam, V.; Ivanov, M. R.; Goodman, A. M.; Haes, A. J. Salt-Mediated Self-Assembly of Thioctic Acid on Gold Nanoparticles. *ACS Nano* **2011**, *5*, 4570−4580.
(30) Wu, G.; Robertson, D. H.; Brooks, C. L.; Vieth, M. Detailed analysis of grid-based molecular docking: A case study of CDOCKER? A CHARMm-based MD docking algorithm. *J. Comput. Chem.* **2003**, *24*, 1549−1562.
(31) Li, D.; Wieckowska, A.; Willner, I. Optical Analysis of Hg2+ Ions by Oligonucleotide−Gold-Nanoparticle Hybrids and DNA-Based Machines. *Angew. Chem., Int. Ed.* **2008**, *47*, 3927−3931.
(32) Wang, J.; Wu, L.; Ren, J.; Qu, X. Visualizing Human Telomerase Activity with Primer-Modified Au Nanoparticles. *Small* **2012**, *8*, 259−264.
(33) Folmer-Andersen, J. F.; Lynch, V. M.; Anslyn, E. V. Colorimetric Enantiodiscrimination of α-Amino Acids in Protic Media. *J. Am. Chem. Soc.* **2005**, *127*, 7986−7987.
(34) Mirri, G.; Bull, S. D.; Horton, P. N.; James, T. D.; Male, L.; Tucker, J. H. R. Electrochemical Method for the Determination of Enantiomeric Excess of Binol Using Redox-Active Boronic Acids as Chiral Sensors. *J. Am. Chem. Soc.* **2010**, *132*, 8903−8905.
(35) Benesi, H. A.; Hildebrand, J. H. A Spectrophotometric Investigation of the Interaction of Iodine with Aromatic Hydrocarbons. *J. Am. Chem. Soc.* **1949**, *71*, 2703−2707.
(36) Fery-Forgues, S.; Le Bris, M. T.; Guette, J. P.; Valeur, B. Ion-responsive fluorescent compounds. 1. Effect of cation binding on photophysical properties of benzoxazinone derivative linked to monoaza-15-crown-5. *J. Phys. Chem.* **1988**, *92*, 6233−6237.
(37) Zhao, C. F.; Diemert, S.; Cann, N. M. Rational optimization of the Whelk-O1 chiral stationary phase using molecular dynamics simulations. *J. Chromatogr. A* **2009**, *1216*, 5968−5978.

DOI: 10.1021/acsami.8b00149
ACS Appl. Mater. Interfaces 2018, 10, 11872−11879